

## Article

# Grassland Mowing Detection Using Sentinel-1 Time Series: Potential and Limitations

Mathilde De Vroey <sup>\*,†</sup>, Julien Radoux and Pierre Defourny

Earth and Life Institute, Université Catholique De Louvain, 1348 Louvain-la-Neuve, Belgium; julien.radoux@uclouvain.be (J.R.); pierre.defourny@uclouvain.be (P.D.)

\* Correspondence: mathilde.devroey@uclouvain.be

† Current address: 2 Croix du Sud bte L7.05.16, 1348 Louvain-la-Neuve, Belgium.

**Abstract:** Grasslands encompass vast and diverse ecosystems that provide food, wildlife habitat and carbon storage. Their large range in land use intensity significantly impacts their ecological value and the balance between these goods and services. Mowing dates and frequencies are major aspects of grassland use intensity, which have an impact on their ecological value as habitats. Previous studies highlighted the feasibility of detecting mowing events based on remote sensing time series, a few of which using synthetic aperture radar (SAR) imagery. Although providing encouraging results, research on grassland mowing detection often lacks sufficient precise reference data for corroboration. The goal of the present study is to quantitatively and statistically assess the potential of Sentinel-1 C-band SAR for detecting mowing events in various agricultural grasslands, using a large and diverse reference data set collected in situ. Several mowing detection methods, based on SAR backscattering and interferometric coherence time series, were thoroughly evaluated. Results show that 54% of mowing events could be detected in hay meadows, based on coherence jumps. Grazing events were identified as a major confounding factor, as most false detections were made in pastures. Parcels with one mowing event in the summer were identified with the highest accuracy (71%). Overall, this study demonstrates that mowing events can be detected through Sentinel-1 coherence. However, the performances could probably be further enhanced by discriminating pastures beforehand and combining Sentinel-1 and Sentinel-2 data for mowing detection.

**Keywords:** grassland; mowing detection; Sentinel-1; backscattering; coherence; land use intensity



**Citation:** De Vroey, M.; Radoux, J.; Defourny, P. Grassland Mowing Detection Using Sentinel-1 Time Series: Potential and Limitations. *Remote Sens.* **2021**, *13*, 348. <https://doi.org/10.3390/rs13030348>

Received: 22 December 2020

Accepted: 15 January 2021

Published: 20 January 2021

**Publisher's Note:** MDPI stays neutral with regard to jurisdictional claims in published maps and institutional affiliations.



**Copyright:** © 2021 by the authors. Licensee MDPI, Basel, Switzerland. This article is an open access article distributed under the terms and conditions of the Creative Commons Attribution (CC BY) license (<https://creativecommons.org/licenses/by/4.0/>).

## 1. Introduction

Grasslands cover some of the largest terrestrial ecosystems. They provide various goods and ecological services, including food production, wildlife habitat, carbon sequestration and water storage. In order to better understand the state and evolution of grasslands, it is crucial to monitor those ecosystems. In most land cover maps, grasslands and other open biotopes are embedded in a broad land cover class [1–4]. They play a crucial role as habitat for biodiversity, but all grasslands cannot be given the same ecological value. Natural grasslands include a large variety of biotopes of high biological value. In agricultural systems grasslands are managed at varying degrees, including semi-natural hay meadows and intensive pastures. Research has repeatedly shown the impacts of grassland use intensification on their ecological value as habitats [5–7]. Identifying different levels of grassland use intensity is of great interest from an agricultural and ecological perspective [8]. Grassland use intensity can be expressed, inter alia, in terms of mowing frequency, grazing intensity and fertilisation. Although these three factors are all important to quantify grassland use intensity in an exhaustive way, individual factors can be related to specific ecological responses, for example, the impact of mowing events on the abundance of some bird species [9].

While in situ terrestrial monitoring methods are often very time consuming, remote sensing can be a great asset for large scale grassland use intensity assessment [8].

Several studies have been carried out on agricultural grassland mapping and monitoring through remote sensing, most of which were based on optical imagery [10–13]. Mowing frequency, grazing intensity and fertilisation input have been estimated using multi-spectral time series (MODIS, RapidEye, Sentinel-2) and agricultural statistics, regionally [14] or at a broader scale [15].

Although some studies focused on grazing intensity [13,14,16], more efforts have been dedicated to detecting mowing events. A mowing event implies a drastic change in a grasslands vegetation cover, as a significant fraction of biomass is removed. Such a change has an impact on the interaction between vegetation and incoming radiation. It should therefore be possible to monitor mowing events by change detection using satellite time series with sufficient spatial and temporal resolutions. In optical remote sensing, mowing events have been associated with drops in normalised difference vegetation index (NDVI) time series, derived from the red and near infrared (NIR) bands [15,17,18] or with changes in red edge vegetation index time series [14].

In order to detect mowing events, it is crucial to ensure a regular and high observation frequency, which can be a challenge when using optical sensors in cloudy regions [19]. In that context, Synthetic Aperture Radar (SAR) imagery presents a great potential, since active radar sensors are independent of sun light and cloud cover. They thus guarantee a continuous coverage over time, making them almost all-weather systems, unlike optical sensors [10,20]. Recent studies have shown the potential of SAR data in applications such as land cover mapping [21] that had been mainly based on optical data in the past. Clear and consistent seasonal patterns have been observed in SAR time series, allowing to detect seeding and harvest dates of several crops [22]. SAR microwaves are influenced by surface geometry and water content [23] among other factors. Harvest activities, such as grassland mowing, change the canopy structure and will thereby influence the radar signal backscattering, along with other factors.

A few studies have evaluated the feasibility of detecting mowing events from SAR imagery, mostly based on backscattering coefficients. The occurrence of a signal rise, followed by a signal decrease in TerraSAR-X backscattering time series, allowed to detect all mowing events in two semi-natural meadows studied by [24]. These encouraging results require to be corroborated on a broader sample. Another study on 34 mown grasslands reported a backscattering increase after mowing events as well [25]. In this study, significant influence of soil water content was observed on the signal. Based on ERS-2 time series, half of the mowing events were detected, while a higher temporal frequency of image acquisition was expected to improve these results. More recently, grassland cutting status was assessed with an 85.7% overall accuracy using artificial neural networks from a set of Sentinel-1 derived variables [26]. It is, however, worth mentioning that the models were trained and tested on just five intensively managed parcels and showed a relatively high false detection rate (25%).

The use of interferometric SAR (InSAR) coherence for detecting mowing events has also been studied. InSAR coherence is a measure of the signal decorrelation between pairs of subsequent SAR acquisitions. Coherence is higher on bare soil and short vegetation than on high grass, because the canopy structure changes over time as grass moves with the wind or gradually grows, causing temporal decorrelation [27–29], while bare soil or short vegetation remain mostly unchanged. After a mowing event, the coherence magnitude of a grassland should rise, as there is less movement in short cut grass. An inverse logarithmic relation has hence been observed between the temporal interferometric coherence and both the vegetation height and the wet above-ground biomass [30]. It has been shown that coherence values are significantly higher after a mowing event, especially when an acquisition is available between 0 and 12 days after the event [31]. On aggregated coherence time series of about 1000 grassland parcels, the authors of [29] observed the typical signature profiles of mowing and ploughing events, showing lower coherence values during the growing phase and high values after the events, as expected in theory. Although the authors of [29,31] identify several confounding factors, such as farming activities or precipitation,

they conclude that mowing detection using C-band SAR interferometric coherence is feasible and encourage further research to evaluate mowing detection accuracy of different methods and identify other confounding factors.

Although providing encouraging results, studies on grassland mowing detection using SAR time series have mainly been carried out on rather limited study areas, covering 2 to 40 grassland parcels [24,31]. In their recent review on remote sensing of grassland production and management, the authors of [32] raise a critical point in grassland mowing detection: the lack of consistent validation data. In many cases, a robust and independent validation data set is missing or lacks sufficient temporal resolution or spatial coverage.

The goal of the present study is to assess the potential of Sentinel-1 C-band SAR for detecting mowing events in various agricultural grasslands in a statistically sound manner, using a large and diverse reference data set. The aim is to answer three questions, namely (1) how accurately can mowing events be detected in grasslands based on Sentinel-1 time series only, (2) what are the main limitations and confounding factors to mowing detection with Sentinel-1 and (3) can Sentinel-1 based mowing detection be used to identify different grassland mowing dynamics? For this purpose, an intensive field campaign was carried out, providing timely information on mowing and grazing events in various grassland parcels. This allowed developing and calibrating several methods, based on the literature and on preliminary observations and to carry out a thorough performance analysis, providing a statistically significant evaluation of Sentinel-1's mowing detection potential.

## 2. Study Area

This study was performed on permanent grasslands in Wallonia, the Southern region of Belgium, covering 16,901 km<sup>2</sup> (Figure 1). Permanent grasslands cover 35% of the utilised agricultural area (UAA) of the Walloon region [33]. Grasslands are defined as permanent in the regional land parcel identification system (LPIS) [34] when no crop rotation has occurred for at least 5 years. The number of parcels and the management intensity vary across the different agro-geographical areas of the region (Figure 1). The delimitation of these areas is based on agro-ecological conditions and cropping systems. The present study encompasses a significant diversity of agro-ecological and farming conditions and includes Condroz, Fagne-Famenne and Ardennes, with respectively about 37%, 71% and 88% of the UAA occupied by grasslands [35]. Other agricultural areas dominated by grasslands include Pays de Herve and Lorraine, which were not covered in this study for field campaign feasibility reasons. This study focuses more precisely on grasslands classified as “E 2.1 Permanent mesotrophic pastures and aftermath grazed meadows” and “E2.2 Low and medium altitude hay meadows” in the European Nature Information System (EUNIS). The first class includes permanent pastures and mixed mowing and grazing management. The second class, which is strictly mown with no grazing activity, has become scarcer over the past decades [36]. The first mowing date differs depending on the grassland management. In most common grasslands, exploitation activities (grazing and/or mowing) start from mid-April. In grasslands of high biological interest, supported by the EU Common Agricultural Policy, mowing is only allowed after 16 June, for flowering purposes, and before 31 October.

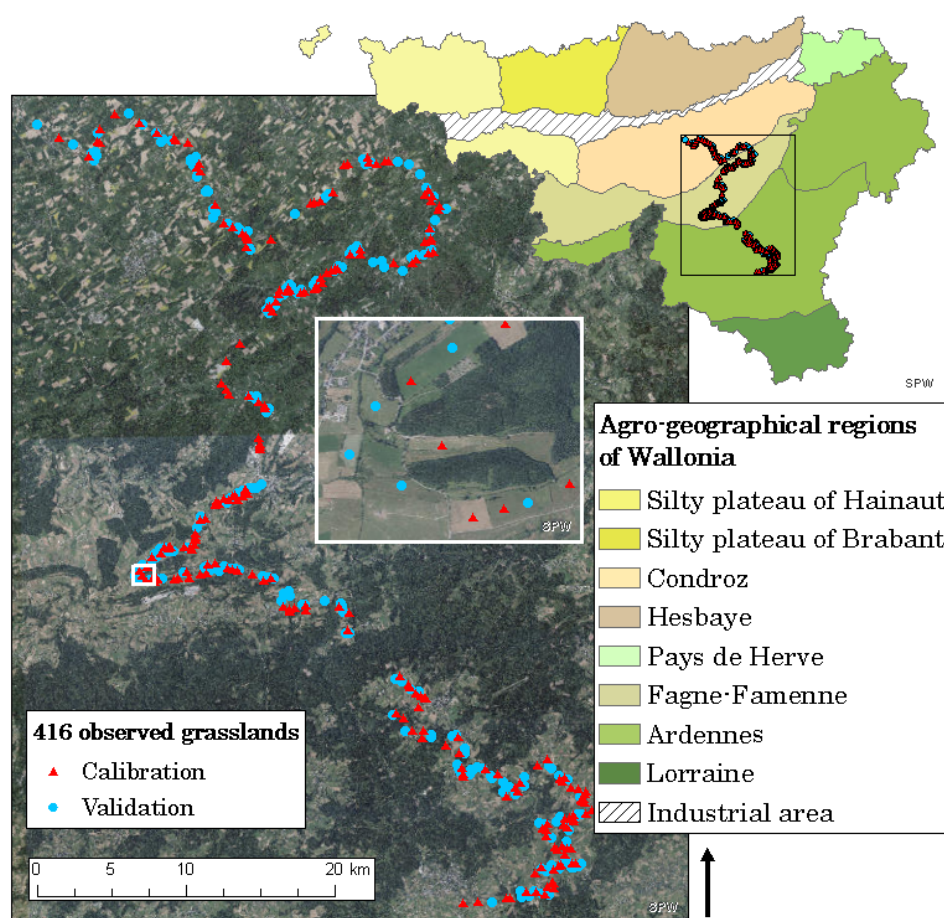


**Figure 1.** Location of the grassland parcels monitored during the windshield survey across 3 main agro-geographical regions of Wallonia (Condroz, Fagne-Famenne and Ardennes). The set of 416 parcels was split in two subsets for calibration and validation of the mowing detection methods.

### 3. Data

#### 3.1. Field Data

An intensive field campaign was carried out to collect reference data for the development, calibration and quantitative performance assessment of mowing detection methods. Between mid-April and mid-July 2019, 11 visits were undertaken on (or near) Sentinel-1 acquisition dates (Figure 2). The campaign was based on a windshield survey throughout the study area. During each visit along the same route, all permanent grasslands were observed from the road and the management status of each parcel was registered as ‘growing’ when no activity could be observed, ‘recently cut’, ‘being cut’ or ‘grazed’ when livestock was present on the parcel. This survey provided information for 10 time intervals on a set of 416 permanent grasslands resulting in a total of 4160 observation intervals. The surveyed grasslands were located in different agro-geographical regions: 76 in Condroz, 190 in Fagne-Famenne and 150 in Ardennes. The field visits were carried out as much as possible at a 6-day pace, corresponding to the Sentinel-1 A and B combined revisit cycle, with the highest frequency in May and June, when the first cuts are expected to occur and the regrowth would be relatively fast. Observations were made with intervals of 6, 12 or 18 days. Overall, 236 mowing events were recorded during the study period. The set of monitored parcels was split into two independent subsets for calibration ( $n = 220$ ) and for validation ( $n = 196$ ) (Figure 1). The subsets were built by stratified random sampling, ensuring that three types of grasslands are represented in each. The first type are parcels in which at least one mowing event was observed but no grazing. They are further referred to as ‘hay meadows’. In the second type, further referred to as ‘mixed practices’, both

mowing and grazing events were observed. In the third type of parcels no mowing events were registered during the study period, but grazing livestock was observed at least once in each. They are further referred to as ‘unmown pastures’.

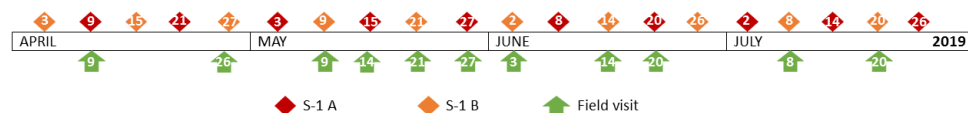


**Figure 2.** Sentinel-1 A and B (descending) acquisition dates over the study area and corresponding field observation dates between April and July 2019.

### 3.2. Sentinel-1 Time Series

Sentinel-1 data was acquired in Single Look Complex (SLC) format and interferometric wide (IW) swath mode with dual polarisation (vertical transmission with vertical reception (VV) or horizontal reception (VH)). The processing to Ground Range Detected (GRD) backscattering coefficient ( $\gamma^0$ ) and interferometric coherence with a 15 m resolution was performed using the Sentinel-1 Toolbox of ESA’s SNAP (version 6.0). The processing chains shown in Figure 3 include calibration, georeferencing, deburst, InSAR coherence estimation (with an averaging window size of azimuth  $\times$  range:  $3 \times 10$ ) and terrain correction. Both chains were run on acquisitions from Sentinel-1 descending pass covering Wallonia during 2019. Only descending pass acquisitions were treated in this study, because coherence should not be computed between different passes (ascending or descending) since the look direction varies. Moreover, field visits were carried out with a minimum interval of 6 days, matching just descending pass acquisition dates, for practical and timely reasons. Coherence was computed between consecutive Sentinel-1 A and B images, in order to reach a 6-day revisit cycle instead of 12, as suggested by [31].

SAR imagery is characterised by an inherent variance (speckle) caused by constructive and destructive interference between randomly distributed scatterers inside a pixel [37]. This speckle effect can be observed on apparent homogeneous surfaces, such as herbaceous covers. In order to spatially smooth the SAR data, the regional LPIS layer [34]—established on an annual basis by the Walloon Administration for the EU Common Agriculture Policy and referencing the localisation, the extent and the main crop of agricultural parcels in Wallonia—was used to average the backscattering and coherence signal per parcel. A 10 m inner buffer was applied to the parcel polygons before averaging, in order to reduce border effects.

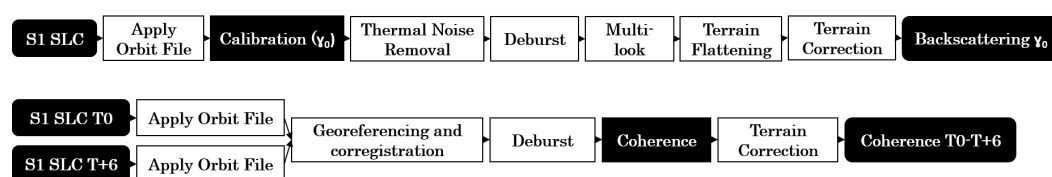


**Figure 3.** Schematic overview of the Sentinel-1 processing chain from single look complex (SLC) interferometric wide (IW) swath mode with dual polarisation (VV, VH) to Ground Range Detected (GRD) backscattering coefficient ( $\gamma^0$ ) and interferometric coherence with a 15 m resolution. Processing performed using the Sentinel-1 Toolbox of ESA’s SNAP (version 6.0).

## 4. Methods

Several mowing detection methods were selected based on previous studies and time series observation, and compared to each other. The methods are based on change detection in time series of a backscattering coefficient on the one hand and of interferometric coherence on the other. All methods were tested using VV and VH signal, as well as a combination of both polarisations, namely the ratio (VV/VH) in the case of backscattering and the average (mean(VV,VH)) in the case of coherence.

#### 4.1. Backscattering Detection Method

This first method, based on  $\gamma^0$  backscattering time series, consists of detecting the occurrence of a signal increase followed by a signal decrease, with respective threshold magnitudes, which have been observed after mowing events in several studies [24,25,38]. The change in backscattering after a mowing event could be linked to a stronger contribution of soil surface scattering, compared to the volume scattering of the vegetation on tall grass. The method selected here is largely based on the two axioms used by [24], namely (1) the occurrence of a signal increase followed by a decrease and (2) the magnitude of those changes above a fixed threshold. For each parcel extracted time series, each value  $\gamma_i$  is compared to the previous  $\gamma_{i-1}$  and the next  $\gamma_{i+1}$ . Two conditions then need to be met.

- (1) The value  $\gamma_i$  needs to be larger than the previous value  $\gamma_{i-1}$  and the next value  $\gamma_{i+1}$ :

$$\gamma_{i-1} < \gamma_i > \gamma_{i+1} \quad (1)$$

- (2) The amplitude of the changes, expressed as per cent increase  $D_{up}$  and decrease  $D_{down}$ :

$$D_{up} = 100 * \left( \frac{\gamma_i - \gamma_{i-1}}{\gamma_i} \right) \quad (2)$$

$$D_{down} = 100 * \left( \frac{|\gamma_{i+1} - \gamma_i|}{\gamma_i} \right) \quad (3)$$

must be higher than the average per cent increase and decrease by a fixed threshold ( $K_{up}\%$  and  $K_{down}\%$ , respectively). The average per cent change describes the signal variation along the entire time series and is computed for each parcel, to be used in the following equations:

$$D_{up} - \frac{\sum_{i=0}^N \frac{|\gamma_i - \gamma_{i-1}|}{\gamma_i} * 100}{N} \geq K_{up}\% \quad (4)$$

and

$$D_{down} - \frac{\sum_{i=0}^N \frac{|\gamma_{i+1} - \gamma_i|}{\gamma_i} * 100}{N} \geq K_{down}\% \quad (5)$$

A detection is made when Equations (1), (4) and (5) are true. This method was tested with different threshold values  $K_{up}\%$  and  $K_{down}\%$  (Table 1).

**Table 1.** Overview of the considered mowing detection methods. The backscattering methods were tested with different input polarisations, per cent increase thresholds ( $K_{up}\%$ ) and different ratios between per cent decrease and increase thresholds ( $K_{down}/K_{up}$ ). The coherence jump detection methods were tested with different polarisations, smoothing approaches, window sizes ( $d$ ) and absolute thresholds (a.t.,  $k$ ) or relative threshold (r.t.) parameters ( $\alpha$ ).

Input	Per Cent Increase Threshold $K_{up}\%$	Ratio ( $K_{down}/K_{up}$ )	
Backscattering ( $\gamma$ ): VV, VH, ratio	2 ; 5 ; 10 ; 15 ; 20 ; 25	1/4 ; 1/2 ; 3/4 ; 1	
Input	Smoothing	Window Size ( $d$ )	Detection Threshold Parameter
Coherence: cohVV; cohVH; cohVVVH	Mean shift	7 ; 9 ; 11	Absolute (a.t) $k= \{0.5, 0.25, 0.1, 0.075, 0.05, 0.025, 0.01, 0.005, 0.0025\}$ ;
	Linear regression	3 ; 4 ; 5 ; 6	Relative (r.t.) $\alpha= \{0.0005, 0.001, 0.005, 0.01, 0.025, 0.05, 0.1, 0.2, 0.4\}$
	Two means	8 ; 10	$p$ -value = $\{0.01, 0.02, 0.03, 0.04, 0.05, 0.06, 0.07, 0.08, 0.09, 0.1, 0.25, 0.5, 0.75\}$

#### 4.2. Coherence Jump Detection Methods

The second set of methods is based on the observation of a high jump in coherence time series right after a mowing event. A mowing event implies a drastic reduction of above ground biomass. According to observations made in previous studies [30,31],

such a reduction in biomass causes a sudden increase from relatively low coherence values to higher ones for a given period of time after the mowing event, before the grass grows tall again. Since coherence tends to fluctuate between consecutive dates despite the spatial filtering, temporal smoothing was applied to reveal significant increases. Based on preliminary observations of coherence time series on various parcels, three jump detection methods implying different smoothing approaches were considered (Figure 4).

**Mean shift:** The first method, called mean shift, consists in a sliding averaging window of a maximum size  $d$  with an adjusting symmetry. It allows to smooth the signal while highlighting significant shifts in the temporal mean such as jumps. When applying the mean shift sliding window, each raw value  $T_i$  is replaced by the average of  $[T_{i-r_1}, T_{i+r_2}]$ , resulting in a smoothed value  $ms(T_i)$ . The number of points before ( $r_1$ ) and after ( $r_2$ ) included in the window are adapted to the local variance of the signal in each window. They are defined by the following limits (Equation (6)) resulting in a maximum window size  $d = 2 * r_{max} + 1$ .

$$\begin{cases} r_1 = r_{max} \\ r_2 = [0, r_{max}] \end{cases} \text{ OR } \begin{cases} r_1 = [0, r_{max}] \\ r_2 = r_{max} \end{cases} \quad (6)$$

Between those limits, the window symmetry parameters  $r_1$  and  $r_2$  adjust for each window to minimize the standard error of the average ( $\sigma_x$ ):

$$\sigma_x = \frac{\sigma_{[T_{i-r_1}, T_{i+r_2}]}}{\sqrt{r_1 + r_2 + 1}} \quad (7)$$

where  $\sigma$  is the standard deviation of  $[T_{i-r_1}, T_{i+r_2}]$ . Jumps are detected between smoothed values when the difference  $ms(T_i) - ms(T_{i-1})$  exceeds a fixed threshold. The method was tested with absolute thresholds (a.t.) ( $k$ ) or relative thresholds (r.t.) to the standard error. In the second case, a Student's test ( $t$ -test) with a given significance level  $\alpha$  is performed. All the tested values for the maximum window size  $d$  and the thresholds  $k$  and  $\alpha$  are summarised in Table 1.

**Linear regression:** In the second method, the time series are smoothed by linear regression using an asymmetrical sliding window. Due to the growth of the vegetation prior to the mowing event, the coherence is expected to gradually decrease and then suddenly increase after the mowing event. In this method, each raw value  $T_i$  is compared to the previous smoothed value  $lr(T_{i-1})$  obtained by linear regression of  $[T_{i-d}, \dots, T_{i-1}, T_i]$ . This allows to consider a potential slope in the coherence profile and detect sudden increases, compared to the previous signal trend. A detection is made when the difference  $T_i - lr(T_{i-1})$  exceeds a given threshold. This method was also tested with different window sizes  $d$ , and absolute ( $k$ ) and relative ( $\alpha$ ) thresholds (Table 1).

**Two means:** The third jump detection method is based on a sliding window of even size  $d$  in which a statistical hypothesis test verifies if there is a significant change in temporal mean coherence in the middle of the window. This is another way to detect a sudden increase in a coherence time series. The null hypothesis  $H_0$  is the approximation by the average value of the whole window  $mean([T_1 : T_d])$ . The alternative hypothesis  $H_1$  is the approximation by a "step model" consisting of two different averages for the first half  $[T_1 : T_{d/2}]$  and second half  $[T_{d/2+1} : T_d]$  of the window. The  $F_{stat}$  used for the test is computed via Equation (8):

$$F_{stat} = \frac{\left( \frac{SSR_0 - SSR_1}{k_1 - k_0} \right)}{\left( \frac{SSR_1}{d - k_1} \right)} \quad (8)$$

where  $SSR_{[0,1]}$  and  $k_{[0,1]}$  are, respectively, the Sum of Squared Residuals and the number of parameters of  $H_{[0,1]}$ . The probability density function of  $F_{stat}$  is derived from  $n$ ,  $k_0$  and  $k_1$  and a  $p$ -value is computed for each date. A  $p$ -value under a given threshold implies a rejection of  $H_0$ . In that case, and if the second mean value is higher than the first, a coherence jump is detected. Table 1 gives an overview of all the coherence jump detection methods applied using the different inputs, window sizes and detection thresholds.

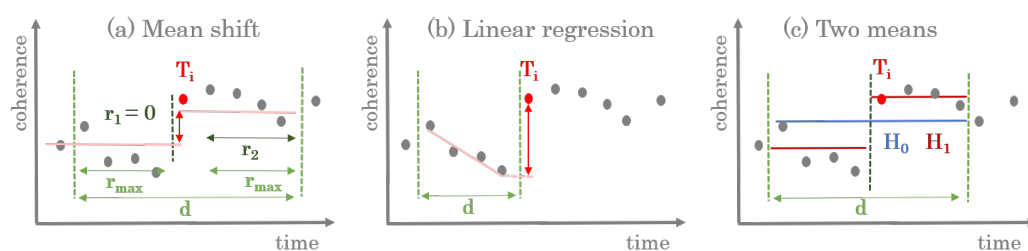


**Figure 4.** Schematic representation of the 3 coherence jump detection methods. A jump occurs at  $T_i$ . (a) The mean shift method with maximum window size  $d = 2 * r_{max} + 1 = 9$  ( $r_1 = 0$  and  $r_2 = r_{max} = 4$ ), where the difference (red arrow) between the smoothed values is evaluated, (b) the linear regression method with window size  $d = 4$ , where raw value  $T_i$  is compared to the previous smoothed value and (c) the two means method of window size  $d = 8$ , comparing the hypothesis  $H_0$  (1 mean) and  $H_1$  (2 means).

#### 4.3. Method Calibration, Evaluation and Validation

The calibration step aimed at identifying the best parameters for each backscattering and coherence jump detection methods, i.e., optimal window sizes and values of the detection thresholds. It was also used to analyse the robustness of these methods to the major confounding factors related to the use of Sentinel-1 data.

The calibrated methods were validated on an independent set of grassland parcels to estimate the potential of Sentinel-1 based mowing detection for identifying different grassland mowing dynamics.

In order to identify optimal parameters, calibration was performed on a subset of the calibration data set with parcels presenting ideal size, shape and slope orientation. Those ideal parcels have an area larger than 1 ha, a width larger than 30 m and the hill shade has to be above the median of the data set. Hill shade was used as indicator for slope orientation, as it is based on the orientation of the slope relative to an illumination source angle and shadows. These three requirements correspond to parcel characteristics potentially affecting the Sentinel-1 signal. Small parcels are expected to be more challenging to monitor because of the limited amount of pixels included in the spatial smoothing. The shape of a parcel could be an issue because narrow parcels might be impaired by border effects (mixed pixels). Finally, the orientation of the slope relative to the radar beam direction will have an impact on the signal interaction with the surface.

The calibrated methods were then applied on parcels presenting less ideal characteristics in order to observe the impact of size, shape and slope orientation on the mowing detection accuracy. In addition to parcel characteristics, the robustness of the methods to grazing activities was assessed. Based on the in situ observations, the data set was split into grazed parcels on which no mowing event was observed, grazed parcels where at least one mowing event was observed and parcels that were mown, but not grazed during the period of observation. These are further referred to as ‘unmown pastures’ ( $n = 105$ ), ‘mixed practices’ ( $n = 36$ ) and ‘hay meadows’ ( $n = 79$ ), respectively.

Quality metrics for calibration and robustness analysis were computed using the time intervals between field visits on each parcel as the unit. There are 10 intervals for each of the 220 parcels selected for calibration, resulting in a total of 2200 observations. Each time interval of each parcel can then be labelled with: the occurrence of mowing event (1) or the absence of mowing event (0), according to field observation and Sentinel-1 mowing detection. Based on the cumulative count of intervals of all parcels, confusion matrices were built between observed and detected mowing events. Since mowing events are relatively rare, there is a strong imbalance between (1) and (0). Therefore, in addition to the broadly used overall accuracy (OA), the Matthews Correlation Coefficient (MCC) was used for calibration and evaluation, along with the sensitivity and precision of mowing detection. The MCC was first introduced by Matthews [39] and the metric is particularly suited to measure the quality of an unbalanced binary classification [40]. The MCC values

range from  $-1$  to  $1$ ,  $0$  being the equivalent of a random classification. The sensitivity is a measure of the detection rate and the precision measures the fraction of detections that are true positives. The MCC metric, the sensitivity and the precision are computed, based on the true (T)/false (F) positives (P) and negatives (N), using Equations (9)–(11).

$$MCC = \frac{TP * TN - FP * FN}{\sqrt{(TP + FP)(TP + FN)(TN + FP)(TN + FN)}} \quad (9)$$

$$Sensitivity = \frac{TP}{TP + FN} \quad (10)$$

$$Precision = \frac{TP}{TP + FP} \quad (11)$$

The best performing and most robust method was then applied to the independent validation data set of 196 parcels. In this case, the performances were evaluated per parcel, instead of per time interval. The aim is to assess the potential of Sentinel-1 based mowing detection methods for identifying different mowing dynamics of grasslands. The assessment was performed for four types of grassland management observed during the field campaign: (i) unmown pastures, (ii) parcels with 1 spring mowing (before 20 June), (iii) with 1 summer mowing and (iv) with 2 mowing events during the study period. For type (i), the potential for identification was assessed by counting the parcels with no detection (identified correctly) and the parcels with at least one false detection. For types (ii) and (iii), the parcels where the mowing event (spring or summer) was detected with no false detection were counted as correctly identified. A further distinction was then made between parcels with false detection, omission or both. Finally, for type (iv), the number of cases in which the two events are detected with no false detection (identified correctly), in which only the first or the second event is detected, in which both are omitted and in which only false detections are made, were counted.

## 5. Results

### 5.1. Method Calibration

All methods were run on the ideal calibration parcels with a range of different detection parameters (Table 1). In total, 12 configurations were considered for methods based on backscattering. For coherence jump detection, 48 different configurations of polarisation, smoothing approach, window size and threshold type were considered. The first observation is that the detection method based on backscattering performed very poorly compared to the coherence jump detection methods. The maximum MCC obtained with backscattering is  $0.25$ , using  $\gamma^0$  VV time series, while the highest MCC values obtained with the different coherence jump detection methods range from  $0.26$  to  $0.49$ . The focus was therefore set on coherence jump detection methods for further analysis.

The different smoothing methods, window sizes and threshold types are compared based on the OA, the sensitivity, the precision and the MCC along the different detection threshold values (Figure 5). The OA (unbroken blue line) reaches high values ranging from  $92\%$  to  $96\%$  for all methods. It drops significantly with low absolute detection thresholds (a.t.), for example, to  $45\%$  for  $k = 0.0025$  with the cohVV linear regression method ( $d = 6$ ), because of the numerous false detections made with such a low detection threshold (Figure 5d).

As expected, when the detection threshold increases ( $1 - \alpha$ ,  $1 - p$ -value and  $k$ ), the precision increases as less false detections occur, but the sensitivity declines as more mowing events are omitted. No significant difference was observed in the shapes of the sensitivity and precision curves, between the different input polarisations (cohVV, coh VH and cohVVVH) or window sizes. On the other hand, the shape of the curves vary from one smoothing method to another as shown in Figure 5. Both with absolute and relative thresholds, the threshold value at which precision and sensitivity reach a balance and the curves cross, is higher for the linear regression method than for the mean shift. For the mean shift

method (Figure 5a,b), when  $\alpha$  tends toward 0 or  $k$  increases, the sensitivity drops relatively low as the detections become more precise. Meanwhile for the linear regression method (Figure 5c,d), the sensitivity remains high with more precise detection thresholds. For the two means smoothing method, the sensitivity also drops relatively fast while the precision does not increase significantly.

The MCC metric (dashed blue line), peaks above 0.4 for all methods except for the two means method (Figure 5e). The two means method was therefore also discarded for further analysis. The MCC peak was used here to select the best performing methods and detection thresholds. However, even at these optimal thresholds, either the precision or the sensitivity are lower than 50% for all methods.

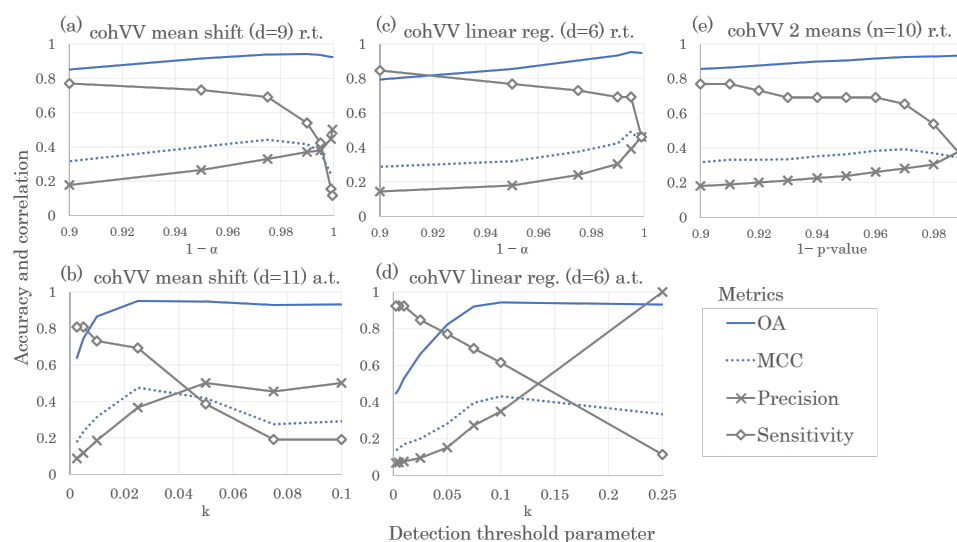


**Figure 5.** Overall Accuracy (OA), Matthews Correlation Coefficient (MCC), precision and sensitivity of several mowing detection methods based on VV coherence, with varying detection threshold parameters. The graphs show the performances of the mean shift and linear regression methods with relative threshold (r.t.) and absolute threshold (a.t.) and of the two means method, with the best window size (d) for each.

For further analysis, the two methods delivering the highest MCC value were selected for VV coherence (cohVV), VH coherence (cohVH) and the average of VV and VH coherence (cohVVVH). The six selected methods are (i) cohVH mean shift ( $d = 9$ ) with relative threshold ( $\alpha = 0.001$ ), (ii) cohVH linear regression ( $d = 5$ ) with r.t. ( $\alpha = 0.0005$ ), (iii) cohVV mean shift ( $d = 11$ ) with a.t. ( $k = 0.025$ ), (iv) cohVV linear regression ( $d = 6$ ) with r.t. ( $\alpha = 0.005$ ), (v) cohVVVH linear regression ( $d = 5$ ) with a.t. ( $k = 0.1$ ) and (vi) cohVVVH linear regression ( $d = 6$ ) with r.t. ( $\alpha = 0.005$ ). The MCC values obtained for these methods range from 0.44 for (ii) to 0.49 for (iv). These calibrated methods are listed in Table 2.

## 5.2. Robustness to Confounding Factors

In order to analyse the robustness of the mowing detection methods, the impact of parcel characteristics on the sensitivity (Sen) and precision (Pre) of the detection was analysed. The results obtained for ideal, small and narrow parcels, for parcels with lower hill shade values, for all non ideal parcels and for all parcels are listed in Table 2.

On the ideal parcels, the calibration based on MCC metrics resulted in a balance between omissions and false detections, depending on the methods. The cohVH mean shift method shows the least balance, with the highest precision (78%) and the lowest sensitivity (27%). The most balanced calibrated method is cohVVVH linear regression with absolute threshold, with a precision and sensitivity of 42% and 54%, respectively. Both methods with VH coherence were calibrated with a higher precision, while the methods with cohVV and cohVVVH resulted in higher sensitivities at the optimal threshold. The highest sensitivity

(69%) on ideal parcels was obtained with both cohVV methods and the cohVH linear regression method with relative threshold.

Among the parcel characteristics the most significant impact is observed for narrow parcels, as both precision and sensitivity are significantly lower for all methods. The largest impact of parcel shape is observed with the cohVH mean shift method, which was also the least balanced. The precision and sensitivity of this method respectively dropped to 13% and 8% on the narrow parcels. The individual effects of size and slope orientation on the accuracy of mowing detection are less significant or consistent through the different methods. Some positive impacts are even observed on the precision.

In order to observe the combined impact of the three parcel characteristics on the sensitivity and precision of mowing detection, ideal and non ideal parcels are compared (Figure 6a). For all methods the sensitivity is lower on non ideal parcels. The effect on the precision is, however, more variable. The most robust methods are cohVH linear regression and both cohVVH linear regression methods, for which the sensitivity and precision vary by less than 10% between ideal and non ideal parcels. For cohVV linear regression, the precision is not impacted by the parcel characteristics, but the sensitivity drops by 20%. As before, the largest impacts are observed on cohVH mean shift, where the precision drops by 31%.

Then the impact of grazing activities on the detection accuracy was assessed, thanks to the observations made during the field campaign (Figure 6b). As expected the sensitivity does not vary when unmown pastures are removed from the data set. The precision is however significantly higher for all methods, namely 64% for cohVVH linear regression with a.t., 72% for cohVV linear regression and 86% for cohVH linear regression, while these methods have precisions of 43%, 42% and 57%, respectively, when considering all types of grasslands. This means that a large part of the false detections was due to unmown pastures. When removing the mixed practices and considering only the hay meadows, the precision and sensitivity barely change and no consistent impact is observed through the different methods.

The most important increase of precision (+30%) after discarding unmown pastures was observed for the cohVV linear regression method ( $d = 6$ ) with r.t. ( $\alpha = 0.005$ ), which has a reasonable sensitivity of 54% on all parcels and reached a 69% detection rate on parcels with ideal characteristics. It was therefore selected as the overall best performing method and used for further parcel-based validation.

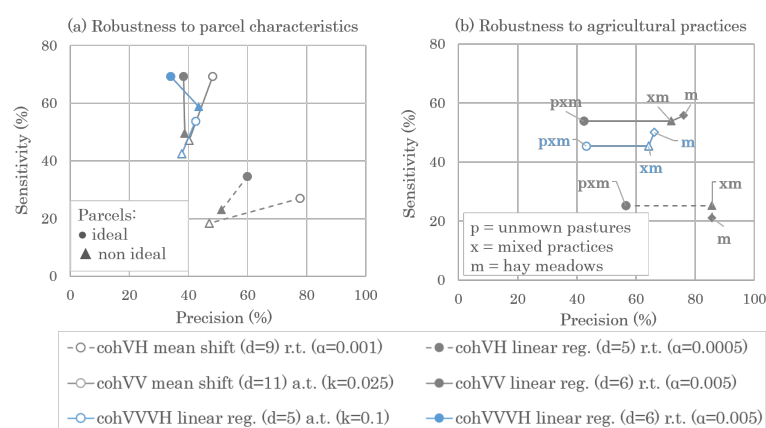


**Figure 6.** Robustness of calibrated Sentinel-1 coherence mowing detection methods to parcel characteristics (size, slope orientation and shape) and grazing practices. Graph (a) shows the changes in precision and sensitivity between detections on large, broad and well oriented parcels (ideal) and on parcels with less ideal characteristics (non ideal). Graph (b) shows the changes in precision and sensitivity when removing unmown pastures (p) and then mixed practices (x), considering hay meadows (m) alone.

**Table 2.** Impact of the size, topography and shape of the parcels on the accuracy of calibrated mowing detection methods, based on VH coherence (cohVH), VV coherence (cohVV) and the average of VV and VH coherence (cohVVH) with absolute (a.t.) and relative (r.t.) threshold and window sizes  $d$ . The threshold parameters  $\alpha$  and  $k$  were optimised based on the Matthews Correlation Coefficient (MCC), to obtain a balance between precision (Pre) and sensitivity (Sen).

	Ideal	Small	Slope Dir	Narrow	Non Ideal	All
<b>n</b>	590	430	770	330	1470	2200
cohVH mean shift ( $d = 9$ ) r.t. ( $\alpha = 0.001$ )						
<b>Pre</b>	78	50	53	13	47	57
<b>Sen</b>	27	8	20	8	18	22
cohVH linear reg. ( $d = 5$ ) r.t. ( $\alpha = 0.0005$ )						
<b>Pre</b>	60	63	59	33	51	54
<b>Sen</b>	35	21	31	15	23	25
cohVV mean shift ( $d = 11$ ) a.t. ( $k = 0.025$ )						
<b>Pre</b>	48	35	44	25	40	42
<b>Sen</b>	69	63	59	31	47	53
cohVV linear reg. ( $d = 6$ ) r.t. ( $\alpha = 0.005$ )						
<b>Pre</b>	38	32	44	32	39	39
<b>Sen</b>	69	42	57	46	49	54
cohVVH linear reg. ( $d = 5$ ) a.t. ( $k = 0.1$ )						
<b>Pre</b>	42	32	44	26	38	38
<b>Sen</b>	54	63	45	46	43	45
cohVVH linear reg. ( $d = 6$ ) r.t. ( $\alpha = 0.005$ )						
<b>Pre</b>	34	46	49	30	44	41
<b>Sen</b>	69	50	67	46	59	61

### 5.3. Parcel-Based Validation

The calibrated cohVV linear regression ( $d = 6$ ) method with r.t. ( $\alpha = 0.005$ ) was applied on the independent validation data set of 196 parcels, for grassland management classification (Figure 7). The aim is to assess the performances for identifying different mowing dynamics of grasslands, based on Sentinel-1 mowing detection.

From the 100 unmown parcels, which were all grazed during the study period, 54% were correctly identified as unmown (first bar of Figure 7), meaning false detections were made in almost half of the unmown pastures. This confirms the results of the robustness analysis, identifying grazing as a major confounding factor to mowing detection with Sentinel-1.

The second bar of Figure 7 shows the performances on the 26 parcels with one spring mowing. Here too, 54% were correctly identified. In the remaining spring mowing parcels the mowing event was omitted and in four parcels (15%) a false detection was made in addition to the omission. Much better results were obtained with summer mowings (third bar of Figure 7), as 71% of the 51 parcels with one summer mowing were correctly identified. A second false detection was made in eight parcels (16%), the summer mowing event was omitted in seven parcels (14%), in two of which a false detection was made in the spring.

Finally, from the 19 parcels with two mowing events (fourth bar of Figure 7), only six (32%) were entirely correct. Here as well, most of the summer events were detected (12 parcels or 64%), while many spring mowings were omitted (nine parcels or 48%). Both mowing events were omitted in only four parcels, one of which also counted as a false detection.

Considering the whole validation data set, 56% of all parcels and 59% of the mown parcels were identified correctly in terms of mowing dynamics, based on Sentinel-1 coherence mowing detection. Most errors consist of false detections in grazed parcels and omitted spring mowing events.

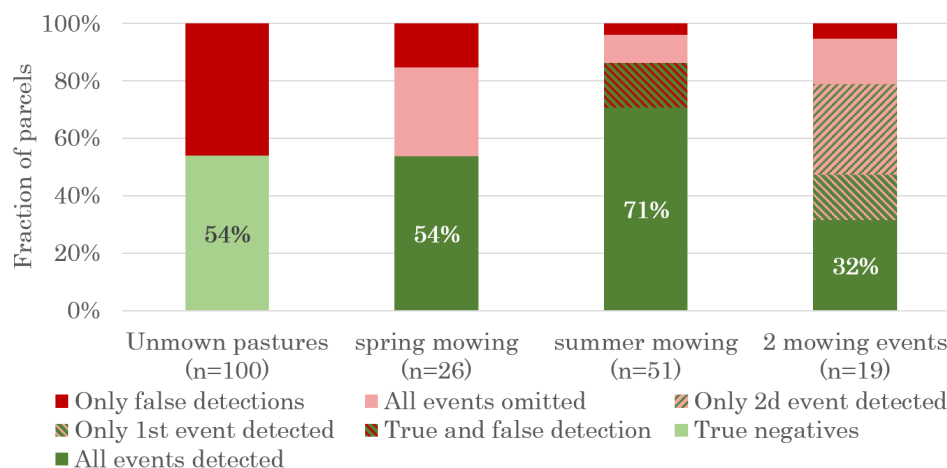


**Figure 7.** Per parcel evaluation of Sentinel-1 VV coherence mowing detection (smoothed by linear regression, with window size  $d = 6$  and relative threshold ( $\alpha = 0.005$ )) potential to identify different mowing dynamics. For each type of dynamic, the fraction of correctly estimated parcels are given, along with the types of errors that occur (false detections, omissions or both).

## 6. Discussion

The results of this study corroborate the potential for detecting mowing events using InSAR coherence, as already suggested by a study on a limited number of grassland parcels [31]. Overall, it was shown that mowing events can be detected by identifying jumps in coherence time series. Based on a large and diverse reference data set, numerous methods could be developed, calibrated and thoroughly analysed on different types of grassland. Once calibrated, most methods showed similar performances and robustness. Nevertheless, the mowing detections based on VV coherence smoothed by linear regression with a window  $d = 6$  and a relative threshold ( $\alpha = 0.005$ ) were slightly more precise and accurate, especially on hay meadows.

### 6.1. Mowing Detection Methods

The methods based on the hypothesis of occurrence of an increase and subsequent decrease in backscattering after a mowing event performed poorly during the calibration phase. The authors of [24] accurately detected all mowing events in two semi-natural meadows, using TerraSAR-X  $\sigma^0$  images, while this study used Sentinel-1 C-band  $\gamma^0$ . Their mowing detection method should therefore be further tested with X-band SAR data on a larger and richer data set.

On the other hand, it was shown that mowing events can be detected by identifying jumps in smoothed coherence time series. The 'two means' smoothing method could be discarded based on lower MCC values, but performances varied little between the different input polarisations, window sizes and detection threshold types for the mean shift and linear regression methods (Table 1). In ideal cases, the mowing event causes such an ample coherence increase that it is easily detected, whatever the method. To the contrary, regardless of the method and parameters, some mowing events cannot be detected at all and coherence jumps can be caused by signal noise or other surface changes. As an illustration, eight coherence time series extracted on different types of parcels, along with the mowing events observed on the field are shown in Figure A1 (Appendix A). Hence, most of the errors are independent of the detection method but inherent to the signal and its interactions with other factors. In order to understand the causes of these

limitations, a robustness analysis was carried out to identify the confounding factors to mowing detection with Sentinel-1 coherence.

### 6.2. Limitations

The sensitivity and precision metrics in Table 2 and Figure 6 show that the size, shape and slope orientation of the parcels can hinder the detection of mowing events for most methods. Fewer mowing events are detected in small or narrow parcels or parcels with a less ideal slope orientation and with some methods, more false detections are made in these less ideal parcels. The differences in accuracy are, however, minor and not always consistent throughout the methods.

From the confounding factors tested in this study, grazing is clearly the most important one. Many false detections were made in parcels that were not mown, but grazed during the study period. During validation, false detections were made in almost half of the unmown pastures, confirming that grazing is a major confounding factor to mowing detection. As coherence increases with decreasing grass height and biomass [30], a grazing event with a large stock density could in fact result in a coherence jump, similar to a mowing event.

In hay meadows and mixed practice parcels, the coherence jump detection method developed in this study allowed to detect most summer mowings, both when they were first or second mowing events, while about half of the spring mowings were omitted (Figure 7). This could be explained by a slower regrowth of the grass after summer cuts, causing the coherence to remain high for a longer period and making the detection easier.

The confounding factors assessed in this study explain some of the false detections and missed mowing events. However, in a number of cases the cause of errors remains unclear. Other factors could hinder the detection of mowing events by impacting the radar signal, such as the presence of trees and shrubs or the soil and plant water content. The impact of water content on radar signal has already been shown previously [23]. It was also shown to be a potential confounding factor to mowing detection [25,31]. In terms of agricultural practices, swaths of grass left on the parcel to dry could also be a confounding factor that alters the signal response after a mowing event.

The mowing detection method developed in this study is object-based and relies on the availability of grassland parcel boundaries for spatial smoothing. The regional LPIS provided this information for this study area. The LPIS parcels are, however, based on farmer declarations, hence partially mown parcels could be a cause for errors. Alternatively, parcel boundaries could be retrieved through automatic delineation based on a convolutional neural network (CNN) [41].

### 6.3. Reference Data and Quality Metrics

The major limiting factor in the development and evaluation of mowing detection methods is the availability of precise and complete field data [32]. The large field campaign carried out in the frame of this study provided information on the land use status of more than 400 agricultural grassland parcels across different agro-geographical regions of Wallonia, on Sentinel-1 acquisition dates. Thanks to this rich data set, it was possible to statistically evaluate the mowing detection potential of Sentinel-1 in agricultural grasslands.

The choice of adequate quality metrics that properly show the performances of a detection method with respect to the context and overarching goal, is another critical point. In the case of the detection of a rare event, the classes of occurrence and absence of the event are unbalanced. Because of that disproportion, the broadly used overall accuracy (OA) is mainly influenced by the numerous absences and is not representative of the detection accuracy. Indeed, the OA reached values above 90% for all methods during calibration, while the detection sensitivity and precision were relatively low (Figure 5). The sensitivity and the precision focus on the true positives, false positives and false negatives and clearly represent the performances of a detection method from the point of view of the events occurrence. Increasing the detection threshold enhances the precision,

but reduces the sensitivity, as more events are omitted. When calibrating the mowing detection methods, a compromise needs to be made between maximising the detection rate and minimising the false detections. In this study, the MCC metric was used to calibrate the methods and select the optimal detection thresholds as it is well adapted for unbalanced binary classifications [40]. Depending on the methods, this resulted in a higher precision or a higher sensitivity and more or less balance between both metrics. In practice, the detection threshold needs to be set according to the context and the motivation for mowing events detection.

#### 6.4. Potential and Prospects

The Sentinel-1 coherence mowing detection method developed in this study allows to detect most summer mowings in hay meadows. However, considering the diversity of grassland types and management dynamics, the mowing detection lacks precision and some mowing events cannot be detected based only on Sentinel-1 coherence.

In order to enhance the precision, it would be a great asset to differentiate grazed parcels from hay meadows beforehand, as most false detections were made in pastures. Previous studies have been discriminating grazed grasslands from hay meadows, based, for example, on backscattering coefficients [25] or vegetation indices derived from optical imagery [14].

In the prospect of grassland use intensity assessment and habitat monitoring, it is critical to be able to detect early spring mowing events with more certainty, in order to differentiate more intensively managed grasslands from extensive grasslands with a higher ecological value. The performances could probably be improved by combining the Sentinel-1 coherence mowing detection, calibrated to obtain a high precision, with an optical method based on decreases in NDVI, such as [15] or [17].

### 7. Conclusions

The main goal of this study was to assess the full potential of Sentinel-1 for detecting mowing events, by estimating the accuracy of mowing detection, identifying the main limitations and confounding factors and finally evaluate the potential for predicting different types of grassland mowing dynamics. Using timely field data on the state and use of 416 grassland parcels, four Sentinel-1-based mowing detection methods were evaluated with various parameter configurations on diverse grasslands. The methods were based on two main observations of SAR signal response to a mowing event, namely the occurrence of a backscattering signal rise and decrease and of an interferometric coherence jump. While the methods based on backscattering showed very low performances, the coherence jump detection methods allowed to accurately detect a majority of mowing events in hay meadows. However, due to the omission of a significant amount of spring mowings and many false detections in pastures, only 56% of grasslands in a fully independent data set were identified correctly in terms of mowing dynamics. The size, shape topography and agricultural practices explain some of the errors, but a part remains uncertain and must be due to other signal interactions. The results of this study confirm that it is feasible to detect mowing events based on coherence jumps. The performances could probably be further enhanced by discriminating pastures beforehand and combining Sentinel-1 and Sentinel-2 data. However, a compromise will always have to be made between sensitivity and precision and the detection threshold needs to be set accordingly, depending on the context and the purpose of mowing detection.

Grassland mowing detection represents a great asset for estimating grassland use intensity in the context of large scale habitat quality monitoring. Methods to detect mowing events should therefore be further studied and developed using large, diverse and precise field data sets.

**Author Contributions:** Formal analysis, M.D.V.; investigation, M.D.V.; methodology, M.D.V.; supervision, J.R. and P.D.; validation, J.R. and P.D.; writing—original draft preparation, M.D.V.; writing—

review and editing, J.R. and P.D. All authors have read and agreed to the published version of the manuscript.

**Funding:** This research is part of the LifeWatch FWB project in the context of the ESFRI and supported by Fédération Wallonie Bruxelles.

**Institutional Review Board Statement:** Not applicable.

**Informed Consent Statement:** Not applicable.

**Data Availability Statement:** Data sharing not applicable. No new data were created or analyzed in this study. Data sharing is not applicable to this article.

**Acknowledgments:** We acknowledge the Walloon Administration for the land parcel identification system (LPIS) layer used as a spatial filter to extract time series per parcel.

**Conflicts of Interest:** The authors declare no conflict of interest.

## Abbreviations

The following abbreviations are used in this manuscript:

EUNIS	European nature information system
GRD	Ground range detected
InSAR	Interferometric SAR
LPIS	Land parcel identification system
MCC	Matthews correlation coefficient
NDVI	Normalised difference vegetation index
OA	Overall accuracy
SAR	Synthetic aperture radar
SLC	Single look complex
UAA	Utilised agricultural area

## Appendix A

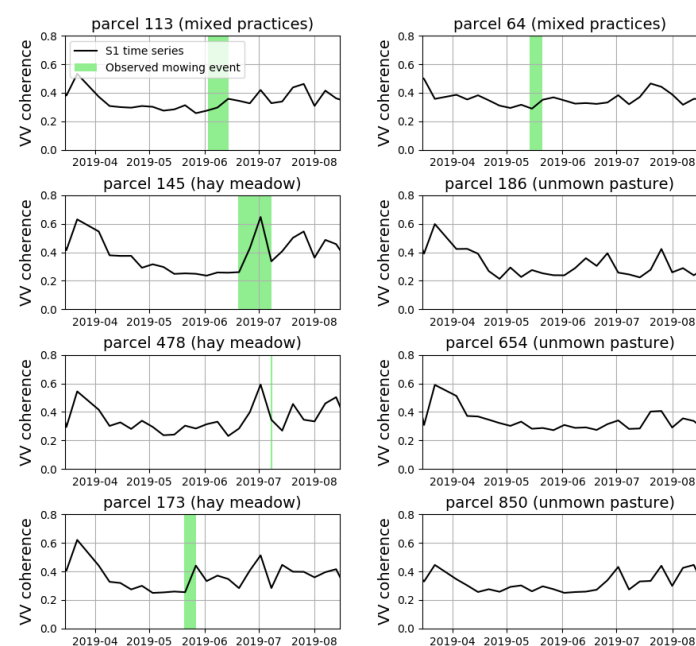


**Figure A1.** Sentinel-1 VV coherence time series extracted from a selection of 8 grassland parcels (2 mixed practices, 3 hay meadows and 3 unown pastures). The green areas represent time intervals in which a mowing event occurred according to field observations. The green line represents a mowing event observed on the day of a field visit.

## References

- Hansen, M.C.; Defries, R.S.; Townshend, J.R.G.; Sohlberg, R. Global land cover classification at 1 km spatial resolution using a classification tree approach. *Int. J. Remote Sens.* **2000**, *21*, 1331–1364. [\[CrossRef\]](#)
- Loveland, T.R.; Reed, B.C.; Brown, J.F.; Ohlen, D.O.; Zhu, Z.; Yang, L.; Merchant, J.W. Development of a global land cover characteristics database and IGBP DISCover from 1 km AVHRR data. *Int. J. Remote Sens.* **2000**, *21*, 1303–1330. [\[CrossRef\]](#)
- Arino, O.; Ramos Perez, J.; Kalogirou, V.; Bontemps, S.; Defourny, P.; Van Bogaert, E. *Global Land Cover Map for 2009 (GlobCover 2009)*; © European Space Agency (ESA) and Université catholique de Louvain (UCL), PANGAEA: Louvain-la-Neuve, Belgium, 2012. [\[CrossRef\]](#)
- Tsendbazar, N.; Herold, M.; Mayaux, P.; Achard, F.; Kirches, G.; Brockmann, C.; Boettcher, M.; Lamarche, C.; Bontemps, S.; Defourny, P. *CCI Land Cover Product Validation and Inter-comparison Report*; Technical Report; UCL-Geomatics: Louvain-la-Neuve, Belgium, 2014.
- Allan, E.; Bossdorf, O.; Dormann, C.F.; Prati, D.; Gossner, M.M.; Tschardt, T.; Blüthgen, N.; Bellach, M.; Birkhofer, K.; Boch, S.; et al. Interannual variation in land-use intensity enhances grassland multidiversity. *Proc. Natl. Acad. Sci. USA* **2014**, *111*, 308–313. [\[CrossRef\]](#) [\[PubMed\]](#)
- Kleijn, D.; Kohler, F.; Baldi, A.; Batáry, P.; Concepción, E.D.; Clough, Y.; Díaz, M.; Gabriel, D.; Holzschuh, A.; Knop, E.; et al. On the relationship between farmland biodiversity and land-use intensity in Europe. *Proc. R. Soc. B Biol. Sci.* **2009**, *276*, 903–909. [\[CrossRef\]](#) [\[PubMed\]](#)
- Uematsu, Y.; Koga, T.; Mitsushashi, H.; Ushimaru, A. Abandonment and intensified use of agricultural land decrease habitats of rare herbs in semi-natural grasslands. *Agric. Ecosyst. Environ.* **2010**, *135*, 304–309. [\[CrossRef\]](#)
- Zlinszky, A.; Schroiff, A.; Kania, A.; Deák, B.; Mücke, W.; Vári, A.; Székely, B.; Pfeifer, N. Categorizing Grassland Vegetation with Full-Waveform Airborne Laser Scanning: A Feasibility Study for Detecting Natura 2000 Habitat Types. *Remote Sens.* **2014**, *6*, 8056–8087. [\[CrossRef\]](#)
- Horn, D.J.; Koford, R.R. Relation of Grassland Bird Abundance to Mowing of Conservation Reserve Program Fields in North Dakota. *Wildl. Soc. Bull.* **2000**, *28*, 653–659.
- Ali, I.; Cawkwell, F.; Dwyer, E.; Barrett, B.; Green, S. Satellite remote sensing of grasslands: From observation to management. *J. Plant Ecol.* **2016**, *9*, 649–671. [\[CrossRef\]](#)
- Asam, S.; Klein, D.; Dech, S. Estimation of grassland use intensities based on high spatial resolution LAI time series. *Int. Arch. Photogramm. Remote. Sens. Spat. Inf. Sci.* **2015**, *XL-7/W3*, 285–291. [\[CrossRef\]](#)
- Dusseux, P.; Vertès, F.; Corpetti, T.; Corgne, S.; Hubert-Moy, L. Agricultural practices in grasslands detected by spatial remote sensing. *Environ. Monit. Assess.* **2014**, *186*, 8249–8265. [\[CrossRef\]](#)
- Franke, J.; Keuck, V.; Siegert, F. Assessment of grassland use intensity by remote sensing to support conservation schemes. *J. Nat. Conserv.* **2012**, *20*, 125–134. [\[CrossRef\]](#)
- Gómez Giménez, M.; de Jong, R.; Della Peruta, R.; Keller, A.; Schaepman, M.E. Determination of grassland use intensity based on multi-temporal remote sensing data and ecological indicators. *Remote Sens. Environ.* **2017**, *198*, 126–139. [\[CrossRef\]](#)
- Estel, S.; Mader, S.; Levers, C.; Verburg, P.H.; Baumann, M.; Kuemmerle, T. Combining satellite data and agricultural statistics to map grassland management intensity in Europe. *Environ. Res. Lett.* **2018**, *13*, 074020. [\[CrossRef\]](#)
- Zheng, J.; Li, F.; Du, X. Using Red Edge Position Shift to Monitor Grassland Grazing Intensity in Inner Mongolia. *J. Indian Soc. Remote Sens.* **2018**, *46*, 81–88. [\[CrossRef\]](#)
- Kolecka, N.; Ginzler, C.; Pazur, R.; Price, B.; Verburg, P.H. Regional Scale Mapping of Grassland Mowing Frequency with Sentinel-2 Time Series. *Remote Sens.* **2018**, *10*, 1221. [\[CrossRef\]](#)
- Griffiths, P.; Nendel, C.; Pickert, J.; Hostert, P. Towards national-scale characterization of grassland use intensity from integrated Sentinel-2 and Landsat time series. *Remote Sens. Environ.* **2020**, *238*, 111124. [\[CrossRef\]](#)
- Sano, E.E.; Ferreira, L.G.; Asner, G.P.; Steinke, E.T. Spatial and temporal probabilities of obtaining cloud-free Landsat images over the Brazilian tropical savanna. *Int. J. Remote Sens.* **2007**, *28*, 2739–2752. [\[CrossRef\]](#)
- Howison, R.A.; Piersma, T.; Kentie, R.; Hooijmeijer, J.C.E.W.; Olff, H. Quantifying landscape-level land-use intensity patterns through radar-based remote sensing. *J. Appl. Ecol.* **2018**, *55*, 1276–1287. [\[CrossRef\]](#)
- Jacob, A.W.; Vicente-Guijalba, F.; Lopez-Martinez, C.; Lopez-Sanchez, J.M.; Litzinger, M.; Kristen, H.; Mestre-Quereda, A.; Ziolkowski, D.; Laval, M.; Notarnicola, C.; et al. Sentinel-1 InSAR Coherence for Land Cover Mapping: A Comparison of Multiple Feature-Based Classifiers. *IEEE J. Sel. Top. Appl. Earth Obs. Remote Sens.* **2020**, *13*, 535–552. [\[CrossRef\]](#)
- Shang, J.; Liu, J.; Poncos, V.; Geng, X.; Qian, B.; Chen, Q.; Dong, T.; Macdonald, D.; Martin, T.; Kovacs, J.; et al. Detection of Crop Seeding and Harvest through Analysis of Time-Series Sentinel-1 Interferometric SAR Data. *Remote Sens.* **2020**, *12*, 1551. [\[CrossRef\]](#)
- Tampuu, T.; Praks, J.; Uiboupin, R.; Kull, A. Long Term Interferometric Temporal Coherence and DInSAR Phase in Northern Peatlands. *Remote Sens.* **2020**, *12*, 1566. [\[CrossRef\]](#)
- Schuster, C.; Ali, I.; Lohmann, P.; Frick, A.; Förster, M.; Kleinschmit, B. Towards Detecting Swath Events in TerraSAR-X Time Series to Establish NATURA 2000 Grassland Habitat Swath Management as Monitoring Parameter. *Remote Sens.* **2011**, *3*, 1308–1322. [\[CrossRef\]](#)
- Curnel, Y. Satellite Remote Sensing Priorities for Better Assimilation in Crop Growth Models: Winter Wheat LAI and Grassland Mowing Dates Case Studies. Ph.D. Thesis, UCL-Université Catholique de Louvain, Ottignies-Louvain-la-Neuve, Belgium, 2015.

26. Taravat, A.; Wagner, M.P.; Oppelt, N. Automatic Grassland Cutting Status Detection in the Context of Spatiotemporal Sentinel-1 Imagery Analysis and Artificial Neural Networks. *Remote Sens.* **2019**, *11*, 711. [CrossRef]
27. Morishita, Y.; Hanssen, R.F. Temporal decorrelation in L-, C-, and X-band satellite radar interferometry for pasture on drained peat soils. *IEEE Trans. Geosci. Remote Sens.* **2014**, *53*, 1096–1104. [CrossRef]
28. Monti-Guarnieri, A.; Manzoni, M.; Giudici, D.; Recchia, A.; Tebaldini, S. Vegetated target decorrelation in SAR and interferometry: Models, simulation, and performance evaluation. *Remote Sens.* **2020**, *12*, 2545. [CrossRef]
29. Voormansik, K.; Zalite, K.; Sünter, I.; Tamm, T.; Koppel, K.; Verro, T.; Brauns, A.; Jakovels, D.; Praks, J. Separability of Mowing and Ploughing Events on Short Temporal Baseline Sentinel-1 Coherence Time Series. *Remote Sens.* **2020**, *12*, 3784. [CrossRef]
30. Zalite, K.; Antropov, O.; Praks, J.; Voormansik, K.; Noorma, M. Monitoring of Agricultural Grasslands With Time Series of X-Band Repeat-Pass Interferometric SAR. *IEEE J. Sel. Top. Appl. Earth Obs. Remote Sens.* **2016**, *9*, 3687–3697. [CrossRef]
31. Tamm, T.; Zalite, K.; Voormansik, K.; Talgre, L. Relating Sentinel-1 Interferometric Coherence to Mowing Events on Grasslands. *Remote Sens.* **2016**, *8*, 802. [CrossRef]
32. Reinermann, S.; Asam, S.; Kuenzer, C. Remote Sensing of Grassland Production and Management—A Review. *Remote Sens.* **2020**, *12*, 1949. [CrossRef]
33. Statbel (Direction générale Statistique—Statistics Belgium). Service Public Fédéral Economie, P.M.E., Classes moyennes et Energie. In *Chiffres clés de l'agriculture 2020*; Statbel (Direction générale Statistique—Statistics Belgium): Brussels, Belgium, 2020.
34. Milionis, N. *The Land Parcel Identification System: A Useful Tool to Determine the Eligibility of Agricultural Land—But Its Management Could Be Further Improved*; Special Report 25; European Court of Auditors: Luxembourg, 2016; doi:10.2865/39118. [CrossRef]
35. Statbel (Direction générale Statistique—Statistics Belgium). Service Public Fédéral Economie, P.M.E., Classes Moyennes et Energie. In *Chiffres clés de l'agriculture 2015*; Statbel (Direction générale Statistique—Statistics Belgium): Brussels, Belgium, 2015.
36. Les prairies et les pelouses (E)—Biotopes—La Biodiversité en Wallonie. Available online: <http://biodiversite.wallonie.be/fr/prairies-et-pelouses-e.html?IDC=815> (accessed on 19 January 2021).
37. Lee, J.; Jurkevich, L.; Dewaele, P.; Wambacq, P.; Oosterlinck, A. Speckle filtering of synthetic aperture radar images: A Review. *Remote Sens. Rev.* **1994**, *8*. [CrossRef]
38. Bargiel, D.; Herrmann, S.; Lohmann, P.; Sörgel, U. Land use classification with high-resolution satellite radar for estimating the impacts of land use change on the quality of ecosystem services. In *100 Years ISPRS Advancing Remote Sensing Science, Pt 1*; International Archives of the Photogrammetry, Remote Sensing and Spatial Information Sciences: Beijing, China, 2010; Volume 38, pp. 68–73; doi:10.15488/1116. [CrossRef]
39. Matthews, B.W. Comparison of the predicted and observed secondary structure of T4 phage lysozyme. *Biochim. Biophys. Acta (BBA)-Protein Struct.* **1975**, *405*, 442–451. [CrossRef]
40. Boughorbel, S.; Jarray, F.; El-Anbari, M. Optimal classifier for imbalanced data using Matthews Correlation Coefficient metric. *PLoS ONE* **2017**, *12*, e0177678. [CrossRef] [PubMed]
41. Waldner, F.; Diakogiannis, F.I. Deep learning on edge: Extracting field boundaries from satellite images with a convolutional neural network. *Remote Sens. Environ.* **2020**, *245*, 111741. [CrossRef]